Applied Physics A (2020) 126:405
https://doi.org/10.1007/s00339-020-03587-2

Applied Physics A
Materials Science & Processing

S.I. : CURRENT STATE-OF-THE-ART IN LASER ABLATION

Two-photon retinal theranostics by adaptive compact laser source

Rok Podlipec[1,2] · Jaka Mur[3] · Jaka Petelin[3] · Janez Štrancar[2] · Rok Petkovšek[3]

Received: 14 October 2019 / Accepted: 27 April 2020 / Published online: 11 May 2020

Abstract
To avoid a devastating effect of eye vision impairment on the information flow from the eye to our brain, enormous effort is being put during the last decades into the development of more sensitive diagnostics and more efficient therapies of retinal tissue. While morphology can be impressively imaged by optical coherence tomography, molecular-associated pathology information can be provided almost exclusively by auto-fluorescence-based methods. Among the latter, the recently developed fluorescence lifetime imaging ophthalmoscopy (FLIO) has the potential to provide both structural information and interacting pictures at the same time. The requirements for FLIO laser sources are almost orthogonal to the laser sources used in phototherapy that is expected to follow up the FLIO diagnostics. To make theranostics more effective and cheaper, the complete system would need to couple at least the modalities of low-power high-repetition-rate FLIO and precision high-pulse energy-adjustable repetition rate phototherapy. In addition, the intermediate-power high repetition rate for two-photon excitation would also be desired to increase the depth resolution. In our work, compact fiber-laser based on high-speed gain-switched laser diode has been shown to achieve adaptable/independently tunable repetition rate and energy per pulse allowing coupled fluorescence lifetime diagnostics via two-photon excitation and phototherapy via laser-induced photodisruption on a local molecular environment in a complex ex vivo retinal tissue.

Keywords Adaptable fiber laser · Retinal tissue · Theranostics · Multimodal imaging · Fluorescence lifetime imaging

1 Introduction

Remarkable progress in the development of advanced retinal diagnostics and therapies has been done in the last decade to provide better sensitivity and specificity for detecting retinal pathologies and to minimize the potential risks for damaging the targeted tissue.

Two large families of diagnostic methods evolved, the first based on detecting retinal fluorescence in the visual part of the spectrum called fundus autofluorescence (FAF) [1, 2] and the second based on the interferometric imaging of retinal layers with NIR light called optical coherence tomography (OCT) [3]. Although, OCT has been developed to an impressive (even 3D) imaging tool [4], its physical background, i.e., interference of the light differently scattered from different tissue structures, hinders more specific identification of the physiologies or pathologies particularly present in the aging retina [5]. On the contrary, FAF being sensitive to the local molecular environment [6] can provide besides morphological more indicative pathology-related information. One of the latest developments based on FAF is fluorescence lifetime imaging ophthalmoscopy (FLIO),

✉ Rok Petkovšek
rok.petkovsek@fs.uni-lj.si

Rok Podlipec
rok.podlipec@ijs.si

Jaka Mur
jaka.mur@fs.uni-lj.si

Jaka Petelin
jaka.petelin@fs.uni-lj.si

Janez Štrancar
janez.strancar@ijs.si

[1] Ion Beam Center, Helmholz Zentrum Dresden Rossendorf (HZDR), Bautzner Landstraße 400, 01328 Dresden, Germany

[2] Jožef Stefan Institute, Jamova cesta 39, 1000 Ljubljana, Slovenia

[3] Faculty of Mechanical Engineering, University of Ljubljana, Aškerčeva 6, 1000 Ljubljana, Slovenia

implemented by Heidelberg Engineering [7–9], or custom FLIO systems [10, 11]. The method can monitor changes in environmental parameters such as recognizing and identifying the early stages of diabetic retinopathy (DR) [8] or age-related macular degeneration (AMD) [12, 13] and can provide metabolic mapping [14] unravelling various macular and retinal diseases [15]. The instrumentation relies on the sub-picosecond pulsed lasers with high repetition rates from few MHz [16] to few tens of MHz [17], encompassing typical rates of mode-locked oscillators and fast detection electronics [18] for FLIO resolution of nearly 100 ps.

Current therapeutic techniques, unlike diagnostics, employ lasers with pulse duration typically orders of magnitude longer, from µs for selective retina therapy (SRT) [19, 20] to ms for pan retinal photocoagulation (PRT) [21]. By low repetition rates and high energy per pulse or fluence (see the schematics in Fig. 1), they provide enough thermal effect for the therapy being effective. However, due to strong absorption on the highly absorbing retinal epithelium, the local dispersion of thermal effects is still rather poorly defined and typically widespread, causing additional complications in adjacent tissue [22]. To better localize the therapeutic effect, laser pulses should in principle be faster, e.g., below µs, but still with enough energy per pulse to deliver efficient therapy. Thus, the technology based on nanosecond laser pulses has been recently developed with already some success in clinical trials to prevent progression of the degeneration processes in AMD [23]. Furthermore, with the development of femtosecond laser technology and its high ability to generate therapeutic effects with markedly less energy per pulse, new possibilities emerged for the modern biomedical field. A few successful clinical therapies have already been applied to corneal eye tissues, where such short pulses can produce various nonlinear, photodisruptive optical effects [24].

To exploit the best of the described diagnostics and therapy approaches, the great challenge in the field still lies in developing the adaptive system combining both diagnostics and adaptive therapy at the same time and not in a sequential way. Such theranostic principle would enable more localized targeting and after-treatment-pulse diagnostics, not being possible with current systems.

The goal of our work was thus to overcome the current limitations of the retinal diagnostic and therapeutic laser sources and boost the development of a more universal laser source concept and its application. One direction is high-power mode-locked fs laser technology (Ti:Sapphire), which was already shown promising for diagnostics with the ability to do two-photon excitation FLIO [11, 15] and could as well be promising for the therapy if enough energy of high repetition pulses is accumulated. However, the lasers lack the flexibility in terms of an adjustable repetition rate to be able to increase energy per pulse needed for efficient therapy and are rather complex, making them particularly expensive.

To address this challenge, we herein present the design and application of the recently developed ps compact fiber laser in near-IR based on a gain-switched laser diode, capable of pre-diagnostics, therapy and post-diagnostics done on ex vivo human retinal samples. The system enables to couple the modalities of low pulse energy high repetition rate (40 MHz) two-photon excitation for diagnostics (FLIO) and high pulse energy low repetition rate (1 kHz) for photodisruptive induced therapy. The laser system has been implemented into the modular nonlinear microscopy setup,

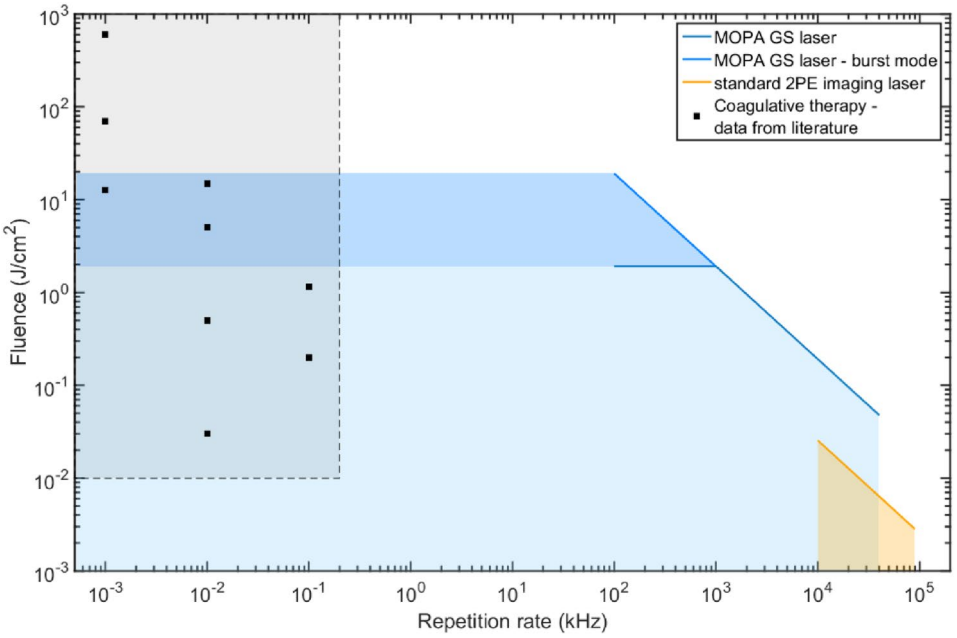

Fig. 1 Laser parameter space. The part of the parameter space of the standard two-photon excitation imaging lasers is denoted with orange line and shade. The data from the literature on laser sources used in photocoagulation therapy [19, 21, 25–31] are denoted with black dots emphasized inside the gray shaded area. Blue lines and shades denote the part of the parameter space covered by the master-oscillator power-amplifier gain-switched fiber laser, with an additional area reached by burst mode operation

allowing near-IR two-photon excitation and fast detection for FLIO.

2 Experimental setups

2.1 Laser source

The master-oscillator power-amplifier (MOPA) gain-switched (GS) fiber laser source, shown in top the right corner of Fig. 2, is a compact all-fiber MOPA where a gain-switched distributed feedback (DFB) laser diode ($\lambda = 1062$ nm) is used to generate laser pulses as short as 65 ps at up to 40 MHz repetition rate [32]. The key parts of the laser system are seed source and especially its driver and fiber-coupled AOM. Seed source driver is capable of generating sub ns electrical pulses with high amplitude (over 50 V) at a high repetition rate. These two parameters (pulse duration and amplitude) are the key in order to achieve a short optical pulse duration (down to 65 ps) while driving standard DFB laser diode. To reach relatively high optical pulse energy, it is required to maintain adequate signal to noise (S/N) ratio of the optical signal in the laser amplifiers chain at a low repetition rate. Another key component is a high-speed electronic circuit that precisely synchronizes and controls both seed driver and AOM as well as the laser pump system. As a result, the laser repetition rate can be set in a broad range from 40 MHz to 1 kHz [33] and the output pulse energy can be set from a few nJ to approximately 15 µJ independently of the repetition rate. The concept allows the laser to operate in a burst mode that includes compensation of the saturation effect appearing in the amplifier chain. Consequently, the energy of almost every individual pulse can be set independently within a certain time slot. Therefore, the high flexibility and beam quality of this laser enable the use of the same laser for diagnostics as well as for therapeutics. While laser systems with equal or even better properties exist, such as Spirit by Spectra-Physics or Pharos by Light Conversion, the complexity of those sources manifests in a higher up-front price and lower reliability compared to the MOPA fiber laser prototype.

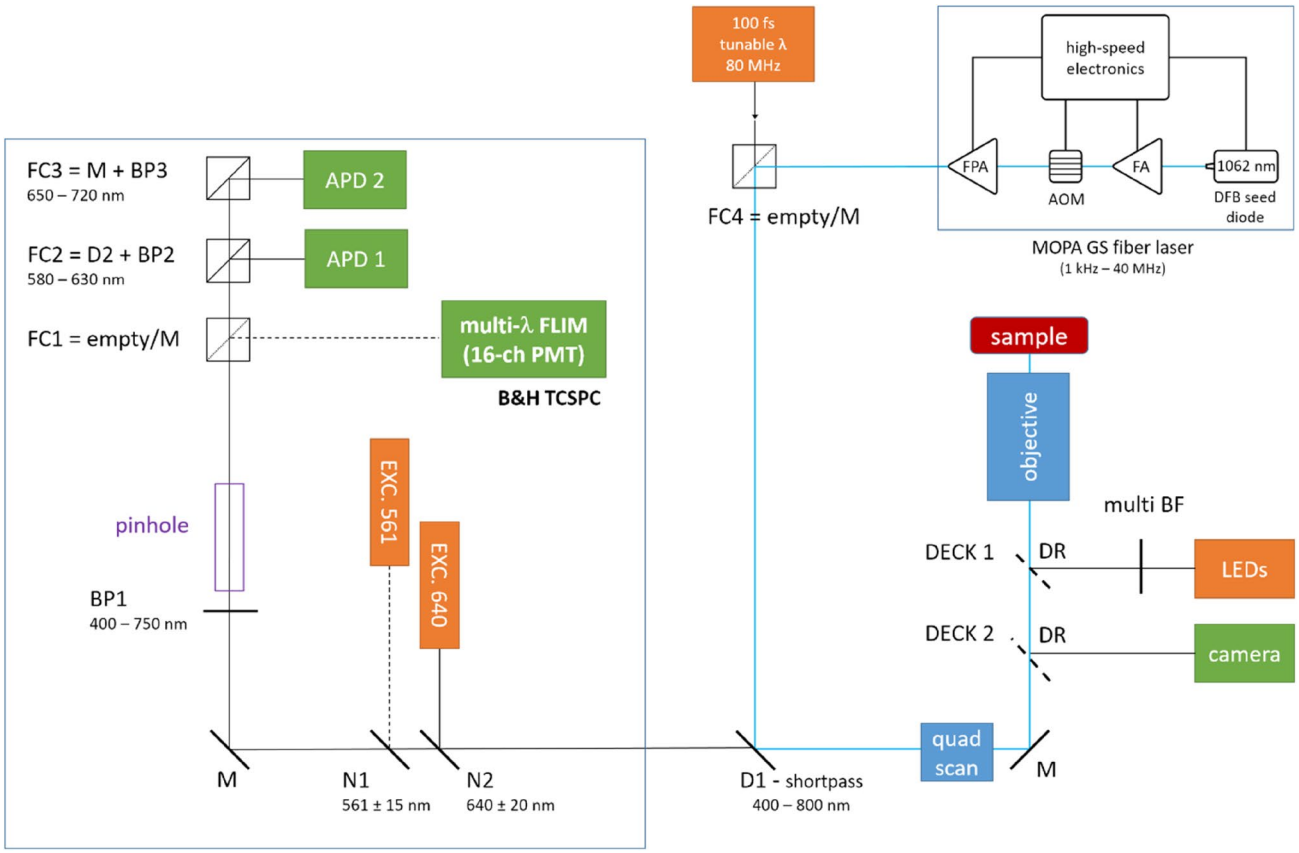

Fig. 2 Scheme of the optical setup. Laser sources are shown in orange color, detection modules in green color. Theranostic study on the ex vivo human retina was mainly focused on using two-photon ps laser source with tunable repetition rate (MOPA GS fiber laser) and multi-channel PMT detector with time-correlated single-photon counter (B&H). *D* dichroic, *DR* dichroic removable, *FC* filter cube, *M* mirror, *BP* bandpass filter, *N* notch filter

2.2 Multi-photon imaging system

A multi-photon multimodal laser-scanning imaging system (Abberior Instruments) was used for ex vivo studies of human retinal tissue (see the schematic on Fig. 2). The compact imaging system is composed of more fluorescence excitation units: one-photon excitation (100 ps pulsed lasers at 561 nm and 640 nm with repetition rate up to 80 MHz and a max output of 200 µW) and two-photon excitation (MOPA GS fiber laser with 65 ps pulse length at 1062 nm with tuneable repetition rate 1 kHz–40 MHz and maximum output power of up to 15 W). Additional femtosecond Ti:Sapphire laser (Chameleon, Coherent) was installed for complementary experiments of two-photon excitation. Various photon counter detectors were used to detect the fluorescence: two avalanche photodiodes (APD, SPCM-AQRH, Excelitas), each for the individual one-photon excitation laser with the fluorescence recording within spectral bands 580–625 nm and 655–720 nm (filters by Semrock), and 16-channel PMT detectors (PML-16-GaAsP, Hamamatsu) accompanied with a time-correlated single-photon counter unit (TCSPC-SPC-150, Becker&Hickl) to acquire additional hyperspectral information of fluorescence decays (tuneable 200 nm range in visible spectra). An additional band-pass filter was mounted to prevent scattered or reflected light entering the detectors. Experiments were performed using a 10× and 60× magnification objectives with the numerical apertures of NA = 0.3 and NA = 1.2 (both Olympus). Images were performed as well with the wide-field illumination using LED source of the wavelength 400 nm and CCD camera. Images using laser scanning system were obtained by fast galvo scanning (Quad Scanner, Abberior Instruments) with a pixel dwell time of max. 10 µs and with more accumulations over predefined scan region in case of low sample signal. Total scan time varied from few seconds to few minutes.

Fluorescence lifetime imaging (FLIM) was recorded with TCSPC [34] synchronized with the laser excitation through fast FPGA communication. The complete fluorescence decay curve was recorded in each image pixel separately. In order to gain a sufficient number of detected counts and thus good S/N ratio, pixel binning had to be used. To obtain a good temporal resolution of the fluorescence decay when low signal counts were detected, we have chosen a conservatively higher binning in order to preserve reasonable spatial resolution. Typical binning when acquiring an image with 256 × 256 pixels and with sufficient signal was set to 2, while in the case of low signal a few times more. The curve fitting using bi-exponential fit was done with software package SPCImage (Becker&Hickl). Fitted parameters were represented with color-coded maps and accompanying histograms. Data are focused on representing the average fluorescence decay time (τ_m).

2.3 Sample preparation

Theranostics studies were performed on ex vivo human retinal tissue. Samples were taken from the enucleated eyes of the patients with severe illness in compliance with national legislation and with the written approval of the patients. Surgical scissors and razor blade were used to separate anterior from the posterior eye segment. The posterior part of an eye excluding vitreous was placed into formalin fixative for 2 h at the room temperature and preserved at 4 °C prior measurements.

3 Results

3.1 Quantification of two-photon excitation capability of MOPA GS fiber laser

To quantify the ability for two-photon excitation to perform diagnostics, a comparison was done with the standard two-photon excitation source (mode-locked Ti:Sapphire laser; Chameleon, Coherent) (Fig. 3, left) using the same near-IR excitation wavelength 1062 nm. The study was performed on the biological sample of the in vitro epithelium model composed of epithelial cell line LA4 labeled with rhodamine B-based membrane probe with good two-photon absorption cross section.

In brief, two-photon excitation is strongly dependent on the peak photon density or photon flux that can be in principal reached by the ultrashort fs to ps laser pulses. Since the electron excitation from the ground to the first excited state is done via an intermediate, very short-lived forbidden energy state, the same molecule must absorb two photons in virtually no time, which demands high photon flux. Based on the generally accepted perception, pulse durations of few tens of ps, typical for our MOPA GS fiber laser, would be considered insufficient for the nonlinear two-photon excitation. However, it can be seen from Fig. 3 that MOPA GS fiber laser (set at a 40 MHz repetition rate) can effectively excite fluorescent molecules by two-photon excitation despite an approximately 10-times lower peak photon density (j) compared to the classical mode-locked fs laser ($t = 100$ fs, $\nu = 80$ MHz). The threshold intensity for two-photon excitation for MOPA GS fiber laser (assuming on 1% of photons detected; N_{counts}/N_{pulses}) was estimated to be approximately $j = 5 \times 10^8$ W/cm^2. The comparison of the experimental parameters between implemented laser systems is shown in the bottom.

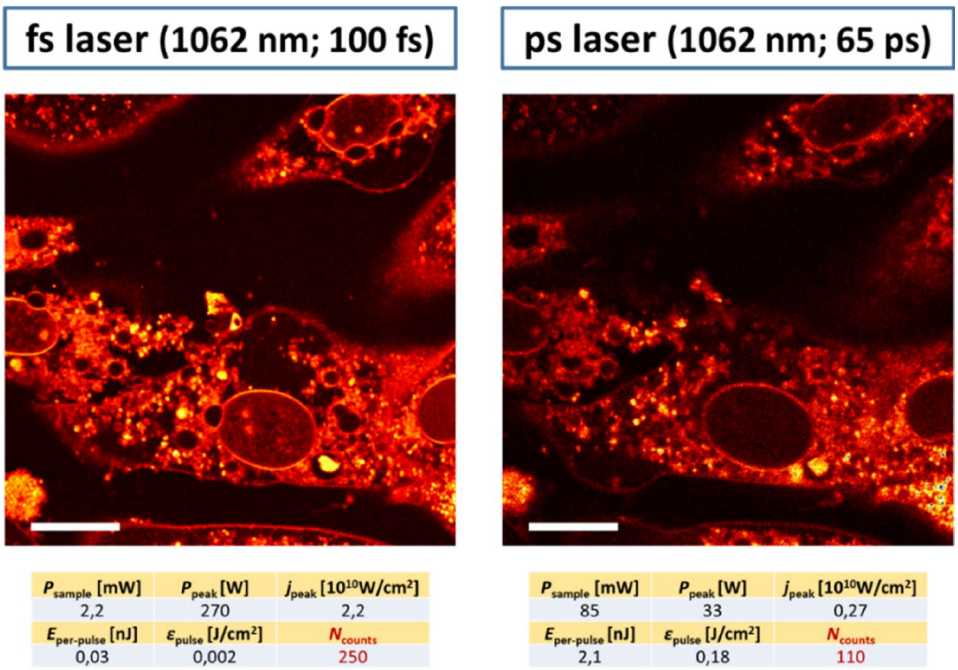

Fig. 3 Quantitative comparison of two-photon excitation using standard fs and MOPA ps pulsed laser on epithelial cells in vitro model labeled with 200 µl 10–5 M rhodamine-based membrane probe. Image size is 500 × 500 pixels with pixel dwell time of 10 µs. Focal plane moved slightly between the two acquisitions measurements. Scale bar is 10 µm

3.2 Quantification of two-photon diagnostics of MOPA GS fiber laser on ex vivo retinal tissue

Since MOPA GS fiber laser was found appropriate for two-photon excitation, we have then tested its applicability on the relevant sample of ex vivo retinal tissue. Besides performing conventional FAF, we have tested the capability of fluorescence lifetime imaging which can provide besides morphological also functional information, essential for any diagnostics.

FLIM analysis was done by fitting the fluorescence decay curve f_m (t) with the convolution integral between the instrument response function (IRF) and the double-exponential decay model f (t):

$$f_m(t) = \int_{\tau=0}^{t} f(t)\mathrm{IRF}(t-\tau)\mathrm{d}\tau$$

$$f(t) = a_1 e^{(-t/\tau_1)} + a_2 e^{(-t/\tau_2)}$$

Relative amplitudes (a_1 and a_2) and the lifetimes (τ_1 and τ_2) of the exponential decay were used to calculate the descriptive mean lifetime τ_m as:

$$\tau_m = \frac{a_1\tau_1 + a_2\tau_2}{a_1 + a_2}$$

As shown in Fig. 4, τ_m decreases significantly at the vessel site, measured both with one-photon as well as two-photon excitation using MOPA GS fiber laser. The corresponding fits of the decay curves on vessel site and surrounding neural retinal tissue are shown in the inset of Fig. 4d. τ_m at vessel site was measured 500 ± 50 ps while in the surrounding neural retinal tissue 1400 ± 100 ps. From the images, one can also see that the τ_m varies across the blood vessel enabling detection of the vessel morphology. Finally, the results nicely show the comparison of the resolution and the sensitivity between one-photon and two-photon excitation.

3.3 Quantification of two-photon diagnostics and therapy of MOPA GS fiber laser on ex vivo retinal tissue

Next, MOPA GS fiber laser has been employed to do subsequent diagnostics and therapy on the same sample site. Theranostics was performed on the retinal epithelial layer (RPE) on two different sites (Fig. 5) with different therapy settings. FLIM-based pre-diagnostics were followed by an adaptive low-frequency operation therapeutic laser targeted to the regions shown within white dotted rectangles. By pre-diagnostics, local regions with lower measured τ_m have been attributed to higher local melanin content (marked with red color) since it is well known that melanin has up to 50% shorter lifetime than surrounding lipofuscin [14]. To perform the therapy, pulse fluence was selected to induce first a noticeable and second, a significant local structural damage (Fig. 5, lower experiment). 40-times higher fluence was needed in comparison with diagnostics pulses that is 0.5 J/cm^2 for first experiment and 1 J/cm^2 for the second. The corresponding pulse energies were 0.1 µJ and 0.2 µJ.

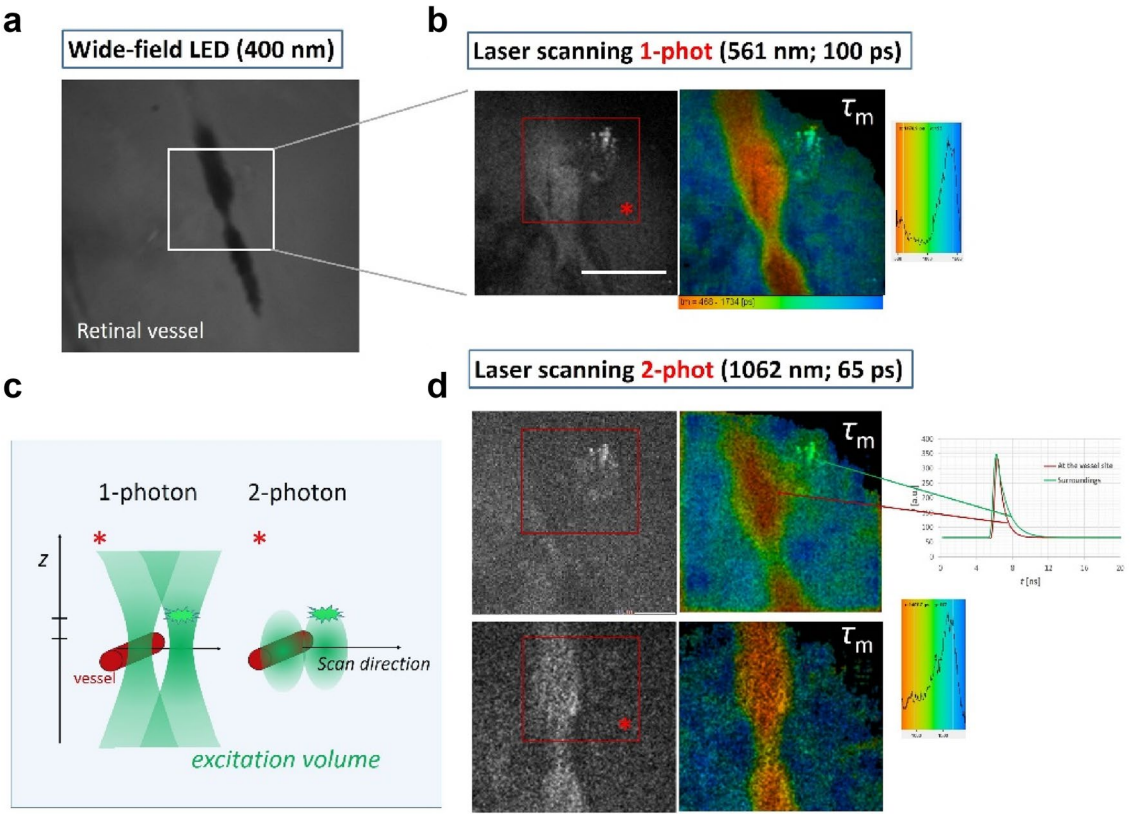

Fig. 4 Comparison of fluorescence lifetime imaging using one-photon and two-photon laser excitation. Better axial resolution was acquired using two-photon MOPA GS fiber laser with a few times lower S/N ratio. **a** The vessel of a fixed ex vivo human retina imaged with wide-field LED illumination. **b** The same region imaged with one-photon (labeled 1-phot) laser scanning showing fluorescence lifetime using PMT detector and TCSPC unit (B&H). **c** Schematics of excitation volumes of one-photon and two-photon laser sources. **d** Two-photon fluorescence lifetime (labeled 2-phot) imaged at different axial planes using MOPA GS fiber laser. The fluorescence lifetime was fitted with two components, τ_m representing the mean lifetime. Laser parameters were $P_{avg} = 50$ µW with 50 MHz repetition rate for one-photon and $P_{avg} = 400$ mW with 40 MHz repetition rate for two-photon. The image resolution is 128 × 128 with 2 µm/pixel. Scale bar is 100 µm

By post-diagnostics analysis, areas that were affected by the therapeutic pulses inside the therapy region have changed structurally as well as functionally shown by FLIM analysis. The difference is more pronounced in the experiment shown in the bottom (Fig. 5, third column). The main changes are seen through the local shifts in τ_m, presented in histograms (Fig. 5, fourth column) and through the partial disappearance of the RPE region, the effect known for a successful selective retinal therapy (SRT) that can be a consequence of either the cell death [35] or the local laser ablation [36].

4 Discussion

The results presented in Fig. 4 nicely show the comparison of two-photon MOPA GS fiber laser with the one-photon diode laser regarding the resolution and the sensitivity. MOPA GS fiber laser can achieve almost the same spatial resolution of the fluorescence lifetime τ_m compared to one-photon excitation (see the vessel region on Fig. 4b, d). However, significantly higher S/N ratio was acquired using one-photon excitation, originating in a much higher photon absorption probability, compared to the two-photon nonlinear process [37]. Thus, the energy of the two-photon laser necessary to acquire relevant FLIM images with the similar sensitivity of retinal vessels was relatively high, but still below the threshold for altering the tissue or the therapeutic effect.

On the other hand, two-photon laser enabled the detection of the retinal structures at higher depths and with better axial resolution (see the marked red region). We could locate the vessel and the nearby pathology clearly at different axial planes, not observed with the one-photon laser, where both structures seem to be in the same axial plane (Fig. 4b, d). This is attributed to more localized excitation volume schematically represented in Fig. 4c.

With both lasers, τ_m at vessel site was measured 500 ± 50 ps while in the surrounding neural retinal tissue

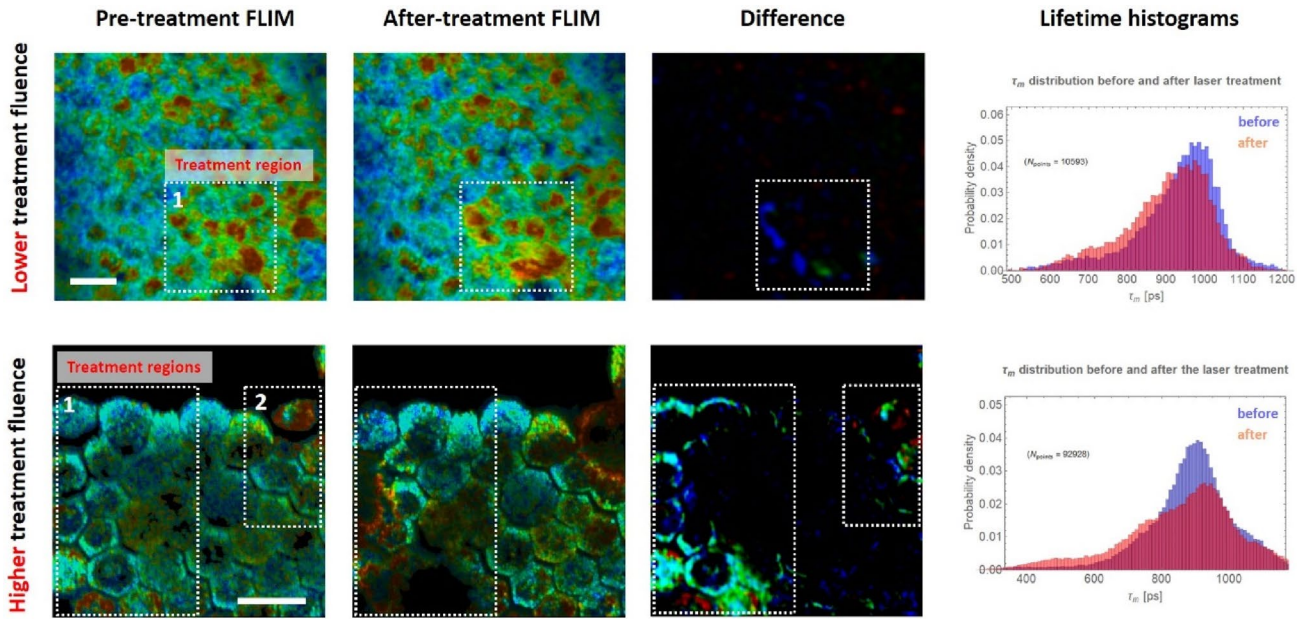

Fig. 5 Diagnostics and therapy of targeted fixed human RPE using the same MOPA GS fiber two-photon laser using low and high magnification objectives. The regions of laser treatment are denoted with white rectangles. The pre- and post-diagnostics were analyzed by calculating τ_m. Sites affected by treatment pulses are clearly visible as seen on the presented difference. The average laser power was the same for diagnostics and treatment ($P_{avg} \approx 100$ mW and $P_{avg} \approx 200$ mW), while the fluence and the energy per pulse were 40-times higher for the treatment ($\varepsilon_{pulse} \approx 0.5$ J/cm^2; $E_{pulse} \approx 0.1$ µJ and $\varepsilon_{pulse} \approx 1$ J/cm^2; $E_{pulse} \approx 0.2$ µJ). The total treatment time at each region was 30 s. The total diagnostics time was 100 s. Scale bar is 20 µm

1400 ± 100 ps. Low τ_m at the vessel site is mainly due to hemoglobin presence which contributes to short fluorescence decay component τ_1, calculated 270 ± 30 ps, which is in a good agreement with the results published recently [38]. Measured lifetime components in the surrounding neural retinal tissue, $\tau_1 = 600 \pm 100$ ps and $\tau_2 = 2500 \pm 300$ ps, on the other hand partially match with the ones in the published data [14]. τ_2 agrees very nicely with the known lifetimes of the most abundant endogenous molecules, such as FAD, collagen and lipofuscin, while τ_1 was measured longer compared to the literature. This could be attributed to changes in the intrinsic fluorescence properties due to chemical fixation that can cause an increase in fluorescence lifetime [39, 40]. However, the fixation of the tissues preserves metabolic contrast, the relationship of the lifetimes and thus the functional information.

The presented applicability of the adaptive MOPA GS fiber laser for retinal diagnostics was further tested for potential applicability in retinal therapy. The results are summarized in Fig. 5, where pre-diagnostics, therapy and post-diagnostics using different modalities of the laser were done on retinal RPE on two different sites with different laser treatment settings. The therapeutic laser parameters were set in such a way to create noticeable (first experiment) to significant structural damage (second experiment). A 40-times higher fluence compared to the diagnostic pulse was needed to induce damage, which was achieved by lowering the laser frequency to 1 MHz. The effect of the increased energy per pulse was observed locally within the chosen treatment region on the few sites with the higher average melanin content than in surroundings.

The local change in τ_m shows that the effect is highly dependent on the local molecular environment, rich in waste material (lipofuscin) and essentially, absorbing melanin specific for retinal pigment epithelium. Furthermore, the effect causes local reduction of the autofluorescence signal as well that was particularly shown for short therapy laser pulses before [35]. Due to the orders of magnitude shorter laser pulses that deliver lower energy doses, a negligible thermal effect was induced as opposed to the known thermal photocoagulation therapies [36]. High peak powers reaching 10^{11} W/cm^2 irradiance rather introduced local plasma mediated ablation [41] on the sites with high melanin content. Melanin can thus indirectly or directly contribute to the changes in fluorescence lifetime—the effect, which has already been documented [42]. It is almost surprising to note that melanin, a complex mixture of different biopolymers derived from tyrosine, known as a broadband absorber, can even express a complex emission decay with fluorescence decay ranging from ps to ns [17]. Another explanation for the decrease in the lifetime in those local regions would be a photodisruptive effect of laser on lipofuscin-rich molecules with longer lifetimes that lose part of the fluorescence.

We have shown that both functional diagnostics using FLIM and local therapy inducing photo-ablation can be done by the same laser source. However, the study was performed on the fixated ex vivo retina, thus questioning the relevance of the used theranostics parameters for in vivo. It was previously shown that fixation can cause a change in the scattering coefficient and retardance to the tissue, but the absorption coefficient remains unchanged [43]. We can thus expect that therapeutic parameters would not be significantly changed when targeting non-fixated tissues.

To sum up, the developed MOPA GS fiber laser has fulfilled several demands for the technology being applicable in future theranostics:

1) Capability of operating at a high repetition rate and sufficient fluence (orange shade of parameter space in Fig. 1) in a controlled, scanning-like approach [44] to collect diagnostics signal in order to localize the following therapeutic pulses (Figs. 4 and 5);
2) Energy per pulse as well as repetition rate were adaptable depending on the mode of action. Diagnostics mode used low power and high repetition rate (orange shade of parameter space in Fig. 1) and in therapy mode vice versa (blue shades of parameter space in Fig. 1);
3) By merging the two modes of action—diagnostics and therapy, the system reduces the need of more sophisticated eye-tracking systems;
4) The system is cost-effective, which is beneficial once introduced into clinics.

5 Conclusions

Compact fiber laser based on high-speed gain-switched DFB laser diode has been shown to achieve adaptable/independently tuneable repetition rate and energy per pulse allowing coupled two-photon fluorescence lifetime diagnostics and photo-induced ablation therapy of local molecular environment in a complex retinal tissue. Several demands for potential applicability in future theranostics were met and discussed thoroughly. This was the first example of implementing a cost-effective adaptive laser source to show efficient simultaneous two-photon-based functional diagnostics and therapy on the relevant human ex vivo retinal sample. However, further laser development is needed before application in clinical trials that could eventually enable advanced theranostics of retinal tissues in vivo.

Acknowledgements The work was primarily carried out in the framework of the GOSTOP program, which is partially financed by the Republic of Slovenia – Ministry of Education, Science and Sport, and the European Union – European Regional Development Fund, as well as in the framework of L7-7561 Project, which is financed by the Slovenian Research Agency ARRS. In addition, this work was also partially supported by other projects of the Slovenian Research Agency ARRS (L2-9240, L2-9254, P2-0270, P1-0060). We would like to acknowledge also the group of prof. B. Drnovšek Olup on the Department of Ophthalmology of the University Medical Clinical Centre Ljubljana to provide us the access to the ex vivo samples of the retinal tissue.

References

1. F.C. Delori, C.K. Dorey, G. Staurenghi, O. Arend, D.G. Goger, J.J. Weiter, In vivo fluorescence of the ocular fundus exhibits retinal pigment epithelium lipofuscin characteristics. Invest. Ophthalmol. Vis. Sci. **36**, 718–729 (1995)
2. A. von Rückmann, F.W. Fitzke, A.C. Bird, Distribution of fundus autofluorescence with a scanning laser ophthalmoscope. Br J Ophthalmol. **79**, 407–412 (1995). https://doi.org/10.1136/bjo.79.5.407
3. A.F. Fercher, K. Mengedoht, W. Werner, Eye-length measurement by interferometry with partially coherent light. Opt. Lett. **13**, 186–188 (1988). https://doi.org/10.1364/OL.13.000186
4. W. Drexler, U. Morgner, R.K. Ghanta, F.X. Kärtner, J.S. Schuman, J.G. Fujimoto, Ultrahigh-resolution ophthalmic optical coherence tomography. Nat. Med. **7**, 502–507 (2001). https://doi.org/10.1038/86589
5. J. Marshall, The ageing retina: physiology or pathology. Eye. **1**, 282–295 (1987). https://doi.org/10.1038/eye.1987.47
6. J. Sparrow, T. Duncker, J.R. Sparrow, T. Duncker, Fundus Autofluorescence and RPE Lipofuscin in age-related macular degeneration. Journal of Clinical Medicine. **3**, 1302–1321 (2014). https://doi.org/10.3390/jcm3041302
7. J. Teister, A. Liu, D. Wolters, N. Pfeiffer, F.H. Grus, Peripapillary fluorescence lifetime reveals age-dependent changes using fluorescence lifetime imaging ophthalmoscopy in rats. Exp. Eye Res. **176**, 110–120 (2018). https://doi.org/10.1016/j.exer.2018.07.008
8. J. Schmidt, S. Peters, L. Sauer, D. Schweitzer, M. Klemm, R. Augsten, N. Müller, M. Hammer, Fundus autofluorescence lifetimes are increased in non-proliferative diabetic retinopathy. Acta Ophthalmol. **95**, 33–40 (2017). https://doi.org/10.1111/aos.13174
9. L. Sauer, R.H. Gensure, M. Hammer, P.S. Bernstein, Fluorescence lifetime imaging ophthalmoscopy: A novel way to assess macular telangiectasia type 2. Oph Retina. **2**, 587–598 (2018). https://doi.org/10.1016/j.oret.2017.10.008
10. D. Schweitzer, L. Deutsch, M. Klemm, S. Jentsch, M. Hammer, S. Peters, J. Haueisen, U.A. Müller, J. Dawczynski, Fluorescence lifetime imaging ophthalmoscopy in type 2 diabetic patients who have no signs of diabetic retinopathy. JBO, JBOPFO. **20**, 061106 (2015). https://doi.org/10.1117/1.JBO.20.6.061106
11. J.A. Feeks, J.J. Hunter, Adaptive optics two-photon excited fluorescence lifetime imaging ophthalmoscopy of exogenous fluorophores in mice. Biomed. Opt. Express. **8**, 2483–2495 (2017). https://doi.org/10.1364/BOE.8.002483
12. C. Dysli, R. Fink, S. Wolf, M.S. Zinkernagel, Fluorescence lifetimes of drusen in age-related macular degeneration. Invest. Ophthalmol. Vis. Sci. **58**, 4856–4862 (2017). https://doi.org/10.1167/iovs.17-22184
13. L. Sauer, C.B. Komanski, A.S. Vitale, E.D. Hansen, P.S. Bernstein, Fluorescence lifetime imaging ophthalmoscopy (FLIO) in eyes with pigment epithelial detachments due to age-related macular degeneration. Invest Ophthalmol Vis Sci. **60**, 3054–3063 (2019). https://doi.org/10.1167/iovs.19-26835
14. D. Schweitzer, S. Schenke, M. Hammer, F. Schweitzer, S. Jentsch, E. Birckner, W. Becker, A. Bergmann, Towards metabolic mapping of the human retina. Microsc. Res. Tech. **70**, 410–419 (2007). https://doi.org/10.1002/jemt.20427
15. C. Dysli, S. Wolf, M.Y. Berezin, L. Sauer, M. Hammer, M.S. Zinkernagel, Fluorescence lifetime imaging ophthalmoscopy.

Progress in Retinal and Eye Research. **60**, 120–143 (2017). https://doi.org/10.1016/j.preteyeres.2017.06.005
16. A. Periasamy, P. Wodnicki, X.F. Wang, S. Kwon, G.W. Gordon, B. Herman, Time-resolved fluorescence lifetime imaging microscopy using a picosecond pulsed tunable dye laser system. Rev. Sci. Instrum. **67**, 3722–3731 (1996). https://doi.org/10.1063/1.1147139
17. A. Ehlers, I. Riemann, M. Stark, K. König, Multiphoton fluorescence lifetime imaging of human hair. Microsc. Res. Tech. **70**, 154–161 (2007). https://doi.org/10.1002/jemt.20395
18. B. Leskovar, C.C. Lo, P.R. Hartig, K. Sauer, Photon counting system for subnanosecond fluorescence lifetime measurements. Rev. Sci. Instrum. **47**, 1113–1121 (1976). https://doi.org/10.1063/1.1134827
19. J. Roider, S.H.M. Liew, C. Klatt, H. Elsner, E. Poerksen, J. Hillenkamp, R. Brinkmann, R. Birngruber, Selective retina therapy (SRT) for clinically significant diabetic macular edema. Graefes Arch Clin Exp Ophthalmol. **248**, 1263–1272 (2010). https://doi.org/10.1007/s00417-010-1356-3
20. E. Seifert, J. Tode, A. Pielen, D. Theisen-Kunde, C. Framme, J. Roider, Y. Miura, R. Birngruber, R. Brinkmann, Selective retina therapy: toward an optically controlled automatic dosing. J Biomed Opt. **23**, 1–12 (2018). https://doi.org/10.1117/1.JBO.23.11.115002
21. S. Al-Hussainy, P.M. Dodson, J.M. Gibson, Pain response and follow-up of patients undergoing panretinal laser photocoagulation with reduced exposure times. Eye **22**, 96–99 (2008). https://doi.org/10.1038/sj.eye.6703026
22. S.V. Reddy, D. Husain, Panretinal Photocoagulation: A Review of Complications. Semin Ophthalmol **33**, 83–88 (2018). https://doi.org/10.1080/08820538.2017.1353820
23. R.H. Guymer, Z. Wu, L.A.B. Hodgson, E. Caruso, K.H. Brassington, N. Tindill, K.Z. Aung, M.B. McGuinness, E.L. Fletcher, F.K. Chen, U. Chakravarthy, J.J. Arnold, W.J. Heriot, S.R. Durkin, J.J. Lek, C.A. Harper, S.S. Wickremasinghe, S.S. Sandhu, E.K. Baglin, P. Sharangan, S. Braat, C.D. Luu, Laser Intervention In Early Stages Of Age-Related Macular Degeneration Study Group, Subthreshold Nanosecond Laser Intervention In Age-Related Macular Degeneration: The LEAD randomized controlled clinical trial. Ophthalmology **126**, 829–838 (2019). https://doi.org/10.1016/j.ophtha.2018.09.015
24. W.R. Calhoun, I.K. Ilev, Effect of therapeutic femtosecond laser pulse energy, repetition rate, and numerical aperture on laser-induced second and third harmonic generation in corneal tissue. Lasers Med. Sci. **30**, 1341–1346 (2015). https://doi.org/10.1007/s10103-015-1726-5
25. Z. Hu, H. Zhang, A. Mordovanakis, Y.M. Paulus, Q. Liu, X. Wang, X. Yang, High-precision, non-invasive anti-microvascular approach via concurrent ultrasound and laser irradiation. Sci. Rep. **7**, 40243 (2017). https://doi.org/10.1038/srep40243
26. J.P.M. Wood, O. Shibeeb, M. Plunkett, R.J. Casson, G. Chidlow, Retinal damage profiles and neuronal effects of laser treatment: comparison of a conventional photocoagulator and a novel 3-nanosecond pulse laser. Invest. Ophthalmol. Vis. Sci. **54**, 2305–2318 (2013). https://doi.org/10.1167/iovs.12-11203
27. Y. Takatsuna, S. Yamamoto, Y. Nakamura, T. Tatsumi, M. Arai, Y. Mitamura, Long-term therapeutic efficacy of the subthreshold micropulse diode laser photocoagulation for diabetic macular edema. Jpn. J. Ophthalmol. **55**, 365–369 (2011). https://doi.org/10.1007/s10384-011-0033-3
28. G. Schuele, H. Elsner, C. Framme, J. Roider, R. Birngruber, R. Brinkmann, Optoacoustic real-time dosimetry for selective retina treatment. JBO, JBOPFO. **10**, 064022 (2005). https://doi.org/10.1117/1.2136327
29. Y.M. Paulus, A. Jain, H. Nomoto, C. Sramek, R.F. Gariano, D. Andersen, G. Schuele, L.-S. Leung, T. Leng, D. Palanker, Selective retinal therapy with microsecond exposures using a continuous line scanning laser. Retina **31**, 380 (2011). https://doi.org/10.1097/IAE.0b013e3181e76da6
30. R.R. Anderson, J.A. Parrish, Selective photothermolysis: precise microsurgery by selective absorption of pulsed radiation. Science **220**, 524–527 (1983). https://doi.org/10.1126/science.6836297
31. W.T. Ham, R.C. Williams, H.A. Mueller, D. Guerry, A.M. Clarke, W.J. Geeraets, Effects of laser radiation on the mammalian eye*†. Trans. N. Y. Acad. Sci. **28**, 517–526 (1966). https://doi.org/10.1111/j.2164-0947.1966.tb02368.x
32. J. Petelin, B. Podobnik, R. Petkovšek, Burst shaping in a fiber-amplifier chain seeded by a gain-switched laser diode. Appl. Opt. **54**, 4629–4634 (2015). https://doi.org/10.1364/AO.54.004629
33. M. Šajn, J. Petelin, V. Agrež, M. Vidmar, R. Petkovšek, DFB diode seeded low repetition rate fiber laser system operating in burst mode. Opt. Laser Technol. **88**, 99–103 (2017). https://doi.org/10.1016/j.optlastec.2016.09.006
34. W. Becker, Advanced Time-Correlated Single Photon Counting Techniques, Springer-Verlag, Berlin Heidelberg, 2005. //www.springer.com/la/book/9783540260479. Accessed September 6, 2018.
35. J.P.M. Wood, M. Plunkett, V. Previn, G. Chidlow, R.J. Casson, Nanosecond pulse lasers for retinal applications. Lasers Surg. Med. **43**, 499–510 (2011). https://doi.org/10.1002/lsm.21087
36. B. Považay, R. Brinkmann, M. Stoller, R. Kessler, Selective Retina Therapy, in *High resolution imaging in microscopy and ophthalmology: New frontiers in biomedical optics*, ed. by J.F. Bille (Springer, Cham, 2019), pp. 237–259. https://doi.org/10.1007/978-3-030-16638-0_11
37. W. Denk, J.H. Strickler, W.W. Webb, Two-photon laser scanning fluorescence microscopy. Science **248**, 73–76 (1990). https://doi.org/10.1126/science.2321027
38. I. Saytashev, R. Glenn, G.A. Murashova, S. Osseiran, D. Spence, C.L. Evans, M. Dantus, Multiphoton excited hemoglobin fluorescence and third harmonic generation for non-invasive microscopy of stored blood. Biomed Opt Express. **7**, 3449–3460 (2016). https://doi.org/10.1364/BOE.7.003449
39. NAD(P)H fluorescence lifetime measurements in fixed biological tissues. - PubMed - NCBI, (n.d.). https://www.ncbi.nlm.nih.gov/pubmed/31553966. Accessed March 17, 2020.
40. D. Schweitzer, E.R. Gaillard, J. Dillon, R.F. Mullins, S. Russell, B. Hoffmann, S. Peters, M. Hammer, C. Biskup, Time-resolved autofluorescence imaging of human donor retina tissue from donors with significant extramacular drusen. Invest. Ophthalmol. Vis. Sci. **53**, 3376–3386 (2012). https://doi.org/10.1167/iovs.11-8970
41. G. Keiser, Light-tissue interactions, in *Biophotonics: Concepts to applications*, ed. by G. Keiser (Springer, Singapore, 2016), pp. 147–196. https://doi.org/10.1007/978-981-10-0945-7_6
42. E. Dimitrow, I. Riemann, A. Ehlers, M.J. Koehler, J. Norgauer, P. Elsner, K. König, M. Kaatz, Spectral fluorescence lifetime detection and selective melanin imaging by multiphoton laser tomography for melanoma diagnosis. Exp. Dermatol. **18**, 509–515 (2009). https://doi.org/10.1111/j.1600-0625.2008.00815.x
43. M.F.G. Wood, N. Vurgun, M.A. Wallenburg, I.A. Vitkin, Effects of formalin fixation on tissue optical polarization properties. Phys. Med. Biol. **56**, N115–N122 (2011). https://doi.org/10.1088/0031-9155/56/8/N01
44. M.A. Mainster, G.T. Timberlake, R.H. Webb, G.W. Hughes, Scanning laser ophthalmoscopy. Clin. Appl. Ophthalmol. **89**, 852–857 (1982). https://doi.org/10.1016/s0161-6420(82)34714-4